Research Square

Preprints are preliminary reports that have not undergone peer review.
They should not be considered conclusive, used to inform clinical practice,
or referenced by the media as validated information.

# Conceptual design of a practical field-reversed configuration magneto- inertial fusion reactor

**B. H. Deng**

bhdeng2002@yahoo.com

Rancho Santa Margarita

**Research Article**

**Keywords:** Magneto-Inertial Fusion, Field-Reversed Configuration, Fusion Reactor, the D-diagram

**Posted Date:** November 13th, 2026

**DOI:** https://doi.org/10.21203/rs.3.rs-11584625/v1

**License:** This work is licensed under a Creative Commons Attribution 4.0 International License.
Read Full License

**Additional Declarations:** Competing interest reported. The author declares that a patent application (application number: 202610481542.8) related to the technology reported in this work has been filed with the patent office.

# Conceptual design of a practical field-reversed configuration magneto-inertial fusion reactor

**B.H. Deng**[1*#]

[1] Independent Researcher, Rancho Santa Margarita, California, USA

*Author to whom any correspondence should be addressed.

#Orcid ID: 0000-0002-7025-2970

**E-mail:** bhdeng2002@yahoo.com

**Keywords:** Magneto-Inertial Fusion, Field-Reversed Configuration, Fusion Reactor, the D-diagram

## Abstract

Magneto-inertial fusion (MIF) is expected to offer the dual advantages of lower cost and a more compact reactor design than both magnetic confinement fusion (MCF) and inertial confinement fusion (ICF). However, existing MIF reactor designs either require destructively high magnetic fields (B. Wang et al., Phys. Rev. E 114, 015211, 2026) or unrealistically long plasma confinement times (T. Nicolas et al., J. Fusion Energy 45:24, 2026) to reach ignition. This article presents a practical MIF reactor design based on acceleration and compression of field-reversed configuration (FRC) plasmas. The most conservative scaling law for FRC plasma confinement time is used to ensure the physics design robustness, and an engineering limit of < 100 T is adopted to enable non-destructive repetitive operation. The unique structural design ensures FRC stability throughout the compression process, and a practical path to ignition is expected at moderate densities (~$10^{24}$ $m^{-3}$). The simple relationship between the minimum required magnetic field for a given confinement time is also presented as "the D-diagram" which can be used as a guide for the design of any fusion reactors with the goal to achieve ignition. The effective kinetic wall compression method used in the design has higher plasma heating efficiency than traditional wall compression and avoids the impurity contamination problem.

## 1. Introduction

The fact that controlled nuclear fusion research is still ongoing after seven decades of worldwide endeavor attests to the challenges in this field, which originate from the extreme conditions required to achieve ignition. One essential condition is the extremely high temperature required. For fusion reactors fueled by deuterium and tritium, the optimum temperature required is ~14.2 keV, or ~160 million degrees Kelvin. In addition, a value of the so-called fusion triple product of plasma density n, ion temperature $T_i$, and energy confinement time $\tau_E$ of $nT_i\tau_E \geq 3\times10^{21}$ keV·s·$m^{-3}$ is required [1].

In magnetic confinement fusion (MCF), the plasma pressure $p = 2nT_i$ is contained by magnetic fields. The containment efficiency $\beta = p/(B^2/2\mu_0)$ is typically ~2%, where $\mu_0$ is the vacuum permeability, and the magnetic field strength B for a modern tokamak design is in the range of 5-12 Tesla [2-4]. This low β characteristic dictates that all MCF devices are low pressure, and consequently low density (~$10^{20}$ $m^{-3}$). Therefore, to reach the critical triple product value it becomes necessary to make the device increasingly larger to achieve longer confinement times. The joint European torus (JET) built in the 1980s with a plasma minor radius of 1.25 m achieved a confinement time of about 0.8s [5,6]. As the next generation tokamak after JET, the International Thermonuclear Experimental Reactor (ITER) has a plasma minor radius of 2.8 m with expected confinement time of 1-4 s [6]. Largely due to the scaled-up size, an MCF reactor is high cost and requires long development time.

Inertial confinement fusion (ICF) experiments are characterized by high density (~$10^{31}$ $m^{-3}$) and short confinement time (~$10^{-10}$ s), which require extremely high heating power to achieve fusion gains [7,8]. This also results in high cost, and the destructively high pressure makes repetitive operation difficult.

Magneto-inertial fusion (MIF) is an emerging controlled fusion approach [9] which integrates the good confinement property provided by magnetic fields with the high pressure provided by modern pulsed power technologies. It is expected to have the advantages of both low cost and compact reactor design compared to MCF and ICF. However, existing MIF reactor designs either require destructively high magnetic fields [10] or unrealistically long field-reversed configuration (FRC) plasma confinement times [11] to achieve ignition. Presented here is a

practical MIF reactor design based on the acceleration and compression of FRC plasmas. In this design, the engineering limit is ristricted to < 100 T to enable non-destructive repetitive device operation [12-16], the FRC tilt stability throughout the compression process is derived from the unique structural design, and ignition is expected at moderate densities (~$10^{24}$ $m^{-3}$) when evaluated with the most conservative FRC confinement time scaling law [17,18]. In the following section, the design logic of the practical MIF reactor is explained, and the advantages of using FRC as the target plasmas are summarized. The details of the new reactor design are presented in section 3, followed by a brief summary in section 4.

## 2. The design logic

### 2.1. The D-diagram

Among the parameters in the triple product $nT_i\tau_E$, the temperature $T_i$ is optimized to be ~14.2 keV [1]. The parameters of choice are plasma density n (or pressure $p = 2nT_i$) or confinement time $\tau_E$. When the confinement time is chosen, the required minimum pressure is determined. Subsequently for a given β, the required magnetic field $B_{min}$ to confine the minimum plasma pressure is determined, as plotted in Fig. 1, which is referred to as the D-diagram. The reverse is also true: for a typical tokamak magnetic field of ~5-12 Tesla [2-4], the required confinement time is ~1-4 s as shown at the lower end of the dashed curve in Fig. 1. This confinement time is long, which dictates that tokamak projects are large scale as confinement time usually scales with the square of the plasma radius. Therefore, a good MIF reactor design should have a plasma density much higher than that in MCF devices so that the required confinement time is lowered significantly [9].

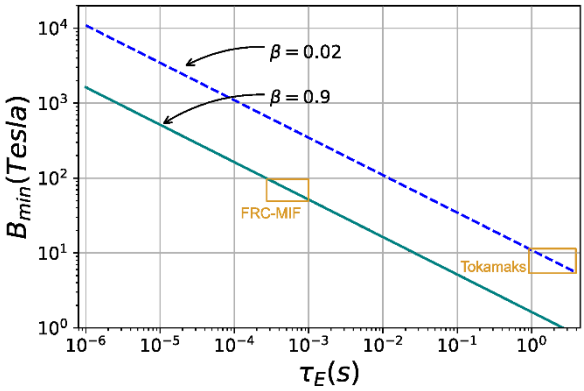



**Fig. 1 Required minimum magnetic field for a fusion reactor to achieve ignition vs the choice of confinement time for given beta values**

In the FRC-based MIF reactor design presented here, there are two factors that can push the density higher. First, a pulsed magnetic field is used in MIF which is about a factor of 10 higher than the steady-state magnetic fields used in tokamaks. Non-destructive pulsed magnets can operate repetitively at a magnetic field of <100 Tesla [12-16]. This can result in a density increase by a factor of about 100.

The other important factor is that FRC plasmas typically have a much higher β of ~0.9 [19], which means that for the same magnetic field, the confined plasma density is 45 times higher than that in MCF devices with β ~ 0.02. This will significantly lower the confinement time requirement, as shown in the solid curve in Fig. 1. It is interesting to see that the FRC confinement time regime of 0.1 – 1 ms overlaps with the non-destructive pulsed magnet operation regime of < 100 T, making it possible to come up with a practical FRC-based MIF reactor design. Before presenting the detailed design, it is necessary to review the advantages of using FRC as the target plasmas.

### 2.2. Advantages of FRC as MIF target plasmas

The first advantage is the simple linear geometry. The plasmas can be generated at one section, and accelerated and compressed at other sections to bring the plasma density and temperature up to fusion conditions. This simple geometry also enables quick replacement of device components that are damaged by neutron irradiation, lowering the component longevity requirement. The second is the higher beta value, which allows a device to operate at higher plasma density for a given magnetic field. In a commercial fusion reactor this can translate to higher economic efficiency. The third is that FRCs are best suited for advanced fusion fuels which allow for high efficiency direct

electricity generation [20]. The fourth is the high efficiency of plasma heating by compression, which is derived from the high beta nature of FRCs. When magnetized plasmas are compressed by an external source, the magnetic field, plasma density and temperature will all increase. The efficiency of work done to heat the plasma in the process of FRC compression is higher compared to that of low beta plasma compression, in which the work is done mostly to compress the magnetic fields. This is a very important advantage for any MIF approaches, since the plasma heating heavily relies on compression. Finally, the fifth advantage is the good confinement property of FRCs. This is partly because FRC plasmas are embedded with closed magnetic field lines. The other reason is related to the simple FRC geometry. Compared to other magnetically confined toroidal plasmas, FRCs do not have a center stack and the plasma gradients on the high field side are flattened, so that the turbulence responsible for anomalous transport is not excited in the plasma core. This is confirmed by numerical simulation [21] and experimental measurements [22]. Typical FRC confinement time is 0.1-1 ms [17-19,23,24], much longer than ~0.1 ns for ICF plasmas, and therefore the heating power requirement is many orders of magnitude less than that required for ICF. This is why it is possible to achieve ignition with existing non-destructive pulsed magnet technology to compress FRC plasma targets.

## 3. The practical FRC-MIF reactor design

### 3.1. FRC parameters to achieve ignition

Past experiments reveal that the FRC plasma energy confinement time follows the empirical scaling law [17,18]:

$$\tau_E = 2.5 \times 10^{-5} \frac{r_s^2}{\rho_{ie}}, \quad (1)$$

where $r_s$ is the separatrix radius, $\rho_{ie} = 1.02\times10^{-4}(A_iT_i)^{1/2}/Z/B_e$ is the ion gyro radius under the external magnetic field $B_e$, $A_i$ is the ion mass number, $T_i$ is the ion temperature (in eV), and Z is the ion charge number. To be able to use non-destructive magnets, the maximum magnetic field is limited to 100 T. From Fig. 1, the corresponding FRC energy confinement time is found to be $\tau_E = 2.68\times10^{-4}$ s. With a temperature of 14.2 keV (when the triple product is at its minimum) $\rho_{ie}$ is calculated to be $1.73\times10^{-4}$ m. From Eq. (1), the FRC separatrix radius is found to be $r_s = 0.043$ m. From the FRC radial force balance $2n_mT_i = B_e^2/2/\mu_0$ [19], the peak plasma density is found to be $n_m = 8.8\times10^{23}$ m$^{-3}$.

The FRC length $l_s$ can be found from the FRC tilt mode stability criterion of $S^*/E \leq 3$ [25], where $S^* = r_s/\lambda_i$, $\lambda_i$ is the ion plasma skin depth, and $E = l_s/2/r_s$ is the FRC elongation. From $\lambda_i \sim 2\rho_{ie}$, $S^*/E$ can be written as

$$\frac{S^*}{E} = \frac{2r_s^2}{l_s\lambda_i} \approx \frac{r_s^2}{l_s\rho_{ie}}. \quad (2)$$

Thus, Eq. (1) can be rewritten as

$$\tau_E \approx 2.5 \times 10^{-5} l_s \frac{S^*}{E}. \quad (3)$$

To achieve a stable FRC with minimum $\tau_E$ of $2.68\times10^{-4}$ s, the minimum FRC length $l_s$ is calculated to be 3.57 m, and the FRC elongation is E = 41.5. This is a significantly higher elongation than typical values of 3-10 reported [19]. The device to realize the FRC design parameters is described below.

### 3.2. The FRC-MIF reactor design

There are three challenges that need to be addressed to achieve the above FRC reactor design parameters for ignition. The first is to form FRC plasmas of sufficiently high density while keeping collisionality low enough that the plasmas can be accelerated and compressed. The second is to make sure that plasma density, temperature, and confinement time can reach the desired values simultaneously. The third is to ensure that the FRC plasma is stable throughout the processes, from the formation stage to the end of the magnetic compression. Shown in Fig. 2 is the schematic of the proposed FRC-MIF fusion reactor design that can overcome these three challenges. High density FRC plasmas with low collisionality are formed in the formation sections at the two ends. They are then accelerated towards the center, then pre-compressed in the conic tubes so that the plasma radius is reduced. In the central section, the FRCs from the two ends collide and merge to form a single FRC, which is then compressed by magnetic fields to achieve the final FRC parameters required for ignition. The unique features of the design are the acceleration section and the metallic conic tube section. The advantages of this design and how the above-mentioned challenges are overcome are explained in the following.

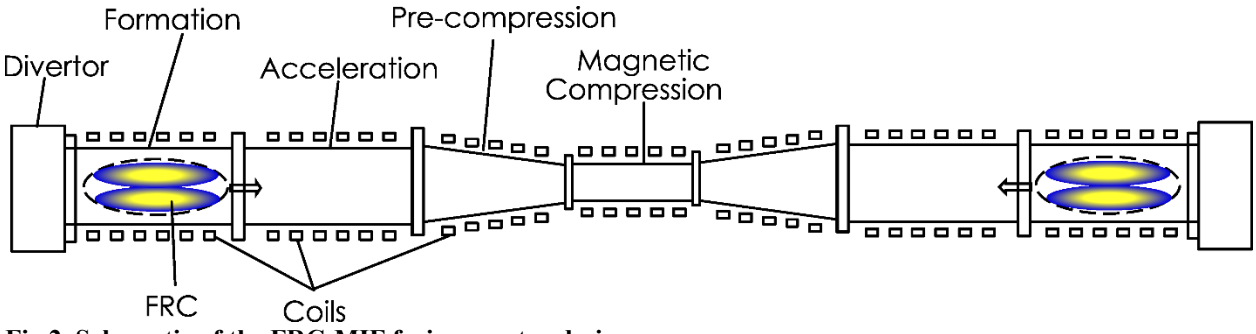



**Fig.2. Schematic of the FRC-MIF fusion reactor design**

### 3.2.1. FRC Formation and acceleration

High FRC plasma density of $10^{23}$ $m^{-3}$ has been achieved in early experiments [26]. However, the total temperature achieved is typically less than 1 keV [26,27] so that the plasmas formed are very collisional with short lifetimes. Physically it is easy to understand that the maximum energy coupled to the plasma by each coil is limited, so that the FRC plasma temperature and axial speed will be lower when the density is higher. A good compromise is to form lower density plasmas and later compress them to higher density. Listed in column 2 of Table 1 are the FRC design parameters in the formation section. These parameters are obtained following the semiempirical model described by Tuszewski [28] and Hoffman [29]. The matured dynamic FRC formation process will be adopted and the axial FRC speed of 250 km/s or less can be achieved [23,30]. Assuming electrons and ions each have half the total temperature, the collision mean free path is calculated to be 0.27 m. This is larger than the FRC radius of 0.195m; therefore, the plasmas can be considered collisionless.

**Table 1. FRC design parameters at each stage, assuming $T_i = T_e = T/2$.**

| Parameters \ Stages | Formed | Accelerated | Merged | Compressed |
|---|---|---|---|---|
| **Coil radius $r_c$ [m]** | 0.26 | 0.26 | 0.12 | 0.12 |
| **Wall radius $r_w$ [m]** | 0.23 | 0.23 | 0.10 | 0.10 |
| **Separatrix radius $r_s$ [m]** | 0.195 | 0.173 | 0.09 | 0.045 |
| **Separatrix length $l_s$ [m]** | 11.55 | 11 | 16.95 | 3.72 |
| **Gas fill pressure $p_0$ [mTorr]** | 33 | - | - | - |
| **Peak density $n_m$ [$10^{21}m^{-3}$]** | 8.85 | 11.9 | 56.9 | 813 |
| **External field $B_e$ [T]** | 1.68 | 2.15 | 9.84 | 96.5 |
| **Total temperature T [keV]** | 0.794 | 0.966 | 4.24 | 28.5 |
| **Mean free path $l_{ei}$ [m]** | 0.27 | 0.29 | 1.2 | 3.75 |
| **$S^*/E$** | 1.9 | 1.85 | 0.7 | 3.0 |
| **Energy confinement time $\tau_E$ [μs]** | 559 | 507 | 301 | 280 |
| **$nT_i\tau_E$ [$10^{21}$keV·s·$m^{-3}$]** | 0.0023 | 0.0029 | 0.026 | **3.02** |

Just as in other FRC experiments, the formation section consists of a quartz tube with surrounding coils distributed along the tube length, and each of the coils are connected to the negative bias, preionization, main reversal, and crowbar circuits [19, 27]. The acceleration section has the same device structure as and works almost identically to the FRC formation section, save for the omission of gas puff and pre-ionization, and the negative bias being changed

into positive forward bias. The bias will provide the basic confinement, and the FRC is accelerated by controlling the timing sequence of the acceleration circuits for each coil to achieve a much higher axial speed. The function of the acceleration section is to accelerate the FRC plasma to a very high speed that has never been achieved before, with two goals. The first goal is to increase the temperature of collisionally merged FRC to a value required for the final flux compression. When two FRCs collide and merge, the kinetic energy effectively changes into thermal energy, which is routinely observed in present FRC experiments [23,24]. When a particle of mass m is moving at a speed v, the kinetic energy is $mv^2/2$. When this is converted into thermal energy upon collision, the resultant temperature T (in eV) is calculated from the following equation:

$$mv^2/2=3T\cdot e/2 \tag{4}$$

Here $e = 1.6\times10^{-19}$ is the electron charge. For Deuterium ions, $m = 2\times1.67\times10^{-27}$ kg. For v = 250 km/s, T is 435 eV. The speed needs to be 760 km/s to obtain a temperature of 4 keV.

The other goal of FRC acceleration is to allow the FRC plasma to travel in the conic metal tube from the larger end to the smaller end, effectively performing FRC wall compression with the gained kinetic energy. Details of this kinetic wall compression process will be explained in the following.

### 3.2.2. FRC compression into the conic tube

The tube in the acceleration section is made of quartz with coils wrapping along the length of the exterior, while the conic tube is metallic with the inside diameter of the entrance end matching that of the quartz tube. The prefilled flux inside the conic tube equals that provided by the coils in the acceleration section. In this transition, the flux conserver radius changes from the coil radius to the conic tube entrance radius. Therefore, the FRC is wall compressed into the conic tube entrance with a compression ratio of the coil radius at the acceleration section of 0.26 m to the conic tube entrance radius of 0.23 m. Listed in column 3 of Table 1 are the parameters when the FRC is compressed at the transition calculated by following the wall compression scalings [31].

### 3.2.3. Free energy of FRC translation

In an FRC translation section, the tube is prefilled with vacuum magnetic field. When the FRC enters the tube, the prefilled flux will be excluded from the volume of the FRC, leading to field line bending and compression outside the FRC. This will increase the system magnetic energy. The total energy of the system will include the plasma thermal energy and the magnetic energy within and outside the FRC. After the FRC moves forward, the prefilled vacuum field will restore. Therefore, the free energy is the total energy minus the vacuum field energy. The total thermal energy and magnetic energy within the FRC volume is derived by Spencer et al. as the following [31]:

$$E_{FRC} = \frac{3}{2} p_m V_{FRC} (1 - {x_s}^2/6), \tag{5}$$

where $p_m = B_e^2/2/\mu_0$ is the peak pressure, $B_e$ is the external magnetic field, $V_{FRC} = \pi r_s^2 l_s$ is the volume of the FRC, $l_s$ is the FRC length, $r_s$ is the FRC separatrix radius, $r_w$ is the radius of the vacuum wall, and $x_s = r_s/r_w$.

Following the same model, the magnetic energy outside the FRC is

$$E_{bo} = \frac{B_e^2}{2\mu_0} \cdot \pi (r_w^2 - r_s^2) l_{FRC} = p_m V_c (1 - x_s^2), \tag{6}$$

where $V_c = \pi r_w^2 l_s$ is the cylindrical wall volume containing the FRC. From the relation between the vacuum field $B_v$ and the external field $B_e = B_v/(1-x_s^2)$, the vacuum field energy is

$$E_{bv} = \frac{V_c B_v^2}{2\mu_0} = p_m V_C (1 - {x_s}^2)^2. \tag{7}$$

From Eqs. (5) to (7), the free energy associated with the FRC (not including the kinetic energy) is

$$E_{free} = E_{FRC} + E_{bo} - E_{bv} = \frac{5}{2} p_m V_{FRC} (1 - x_s^2/2). \tag{8}$$

The conic tube has a metallic wall and is assumed to be prefilled with constant flux so that when the FRC is travelling inside the tube, it undergoes the equivalent of wall compression. As the tube radius becomes smaller, the free energy (including the thermal and magnetic energy) increases. The magnetic field does not do work to the FRC; therefore, the FRC needs to be accelerated to gain sufficient kinetic energy for the expense during compression. With

a certain FRC equilibrium, the total mass $m_p$ can be calculated. Assuming the FRC is accelerated to an initial speed of $v_0$, the sum of the free energy and kinetic energy will be conserved:

$$E_{free,0} + \frac{1}{2} m_p v_0^2 = E_{free,z} + \frac{1}{2} m_p v_{FRC}^2. \quad (9)$$

### 3.2.4. Pre-compression along the conic tube

After acceleration, the FRC is fed into the conic tube for pre-compression. Constant flux equaling to that provided by the coils in the formation and acceleration section is prefilled in the conic tube, so that the FRC is considered to be compressed by wall when entering and traveling in the conic tube from the end with larger diameter. The compression is done with the kinetic energy gained from acceleration. Along the tube with increasing z coordinate, the FRC length, density, temperature, and the magnetic field will vary as the radius decreases following the scalings derived in [31]. $E_{free,z}$ can thus be calculated as a function of z from Eq. (8). From the FRC equilibrium the plasma mass is calculated with Deuterium isotope mass, so that the speed $v_{FRC}$ along the tube can be calculated from Eq. (9). Plotted in Fig. 3 are the normalized variations of plasma peak density, external magnetic field, and total temperature along the conic tube, respectively. The initial parameters at the conic tube entrance are: peak density $n_0 = 1.19\times10^{22}$ $m^{-3}$, total temperature $T_0 = 966$ eV, separatrix radius $r_{s0} = 0.173$ m, entrance wall radius $r_{w0} = 0.23$ m, exit wall radius $r_{w1} = 0.12$ m, and the initial FRC speed $v_0 = 800$ km/s. The maximum values for the normalization are taken at the end of the conic tube with $B_e = 7.9$T, $n_m = 5.7\times10^{22}$ $m^{-3}$, and T = 2.74 keV, respectively. Shown in Fig. 4 is the variation of the FRC speed along the conic tube. From Figs. (3) and (4), it is seen that the increase of plasma thermal energy is at the expense of the kinetic energy, indicated by the decrease of $v_{FRC}$. At the end of the conic tube, $v_{FRC} = 465$ km/s. After exiting the conic tube, the residual kinetic energy is converted into thermal energy in the FRC collisional merging process. The resultant plasma parameters are listed in column 4 of Table 1. From recent numerical studies [32], the fully merged FRC length is the sum of the two original FRC lengths.

As seen in Fig. 3, when FRC plasmas are compressed, the changes in plasma density and temperature follow their own respective scalings [31]. This is also true for magnetic (flux) compression as will be shown in the next section. Therefore, it is important to control the initial values of both the density and temperature before the final compression so that they can reach the design values simultaneously. The density is controlled in the formation section by adjusting the gas filling pressure $p_0$. The acceleration section enables the fine control of the plasma temperature. Dynamically formed high density FRC plasmas have limited axial speed of < 250 km/s for deuterium plasmas, and the maximum ion temperature converted from the kinetic energy by collisional merging is < 435 eV. As will be seen later, the required initial temperature before the final magnetic compression is > 4 keV, and this can be achieved if the FRCs are further accelerated to a speed of >760 km/s in the acceleration section.

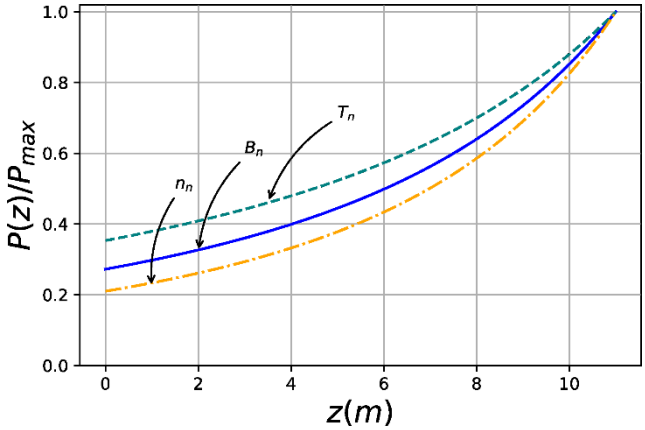



**Fig.3. Variation of external magnetic field $B_e$ (solid curve), peak density $n_m$ (dot-dash curve) and total temperature T (dashed curve) normalized to their respective maxima under wall compression when traveling along the metallic conic tube, the maximum values are $B_e = 7.9$T, $n_m = 5.7\times10^{19}$ $m^{-3}$, and T = 2.74 keV, respectively**

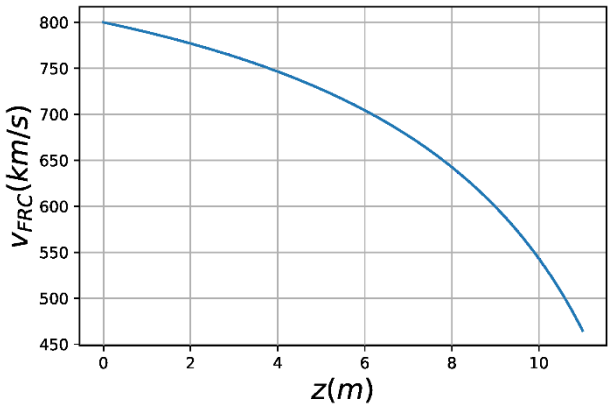



**Fig. 4. Variation of the FRC speed along the conic tube**

### 3.2.5. Flux compression to ignition

After the FRC merging, flux compression is performed so that the plasma density and temperature are increased simultaneously to the values required for ignition. The normalized density, temperature, and external field under flux compression from $x_s = 0.75$ to 0.37 are plotted in Fig. 5, where $x_s = r_s/r_c$ is the normalized FRC radius. These curves are calculated using the flux compression scalings in [31]. The final parameters are listed in column 5 of Table 1, which are close to the parameters prescribed in section 3.1 from simple logical reasoning. Note that iteration processes are performed to achieve the consistent sets of parameters listed in Table 1.

With the empirical FRC confinement time scaling of Eq.(1), the final $nT_i\tau_E$ after flux compression has achieved the ignition critical value of $3\times10^{21}$keV·s·m$^{-3}$ as shown by the solid curve in Fig. 6. This estimate is rather conservative, as collisionally merged FRCs (without neutral beam injection or edge biasing) can have a factor of 2 improvement in confinement time over the scaling of Eq. (1) [17,18]. The dashed curve follows a more optimistic confinement time scaling recently published by Slough [33,34], which leads to almost a factor of 9 improvement in the triple product at the compressed state.

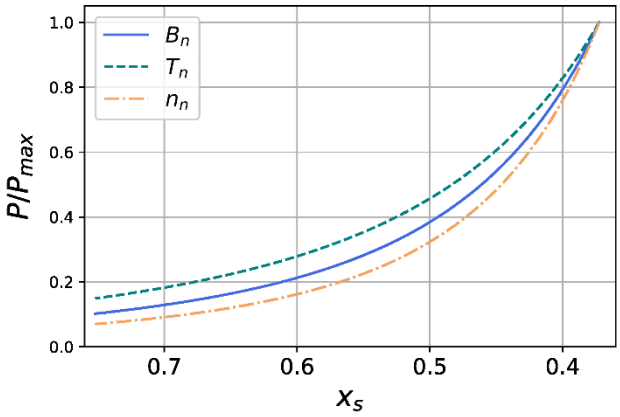



**Fig.5. Variation of external magnetic field $B_e$ (solid curve), peak density $n_m$ (dot-dash curve), and total temperature T (dashed curve), normalized to their respective maxima under flux compression from $x_s = 0.75$ to 0.37 in the central device section. The maximum values of each parameter are listed in column 5 of Table 1**

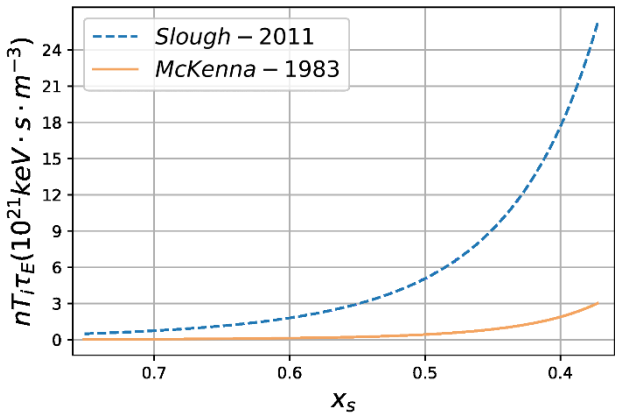



**Fig. 6. The fusion triple products of $nT_i\tau_E$ in the final magnetic compression process. The legends indicate the confinement scalings used**

### 3.2.6. FRC stability control

In addition to achieving the ignition plasma parameters, it is also essential to control the FRC plasma stability for a practical fusion reactor design. Experiments [17, 24] and numerical simulation [35] have shown that the n=1 tilt instability can develop in a very short time scale, while the n=2 and other unstable modes usually develop a few hundred micro-seconds later. For an MIF fusion reactor, the main instability to consider is the n=1 tilt mode, since the FRC formation, acceleration, and compression cycle will be finished in less than 0.1 ms, before the other unstable modes have a chance to develop. Therefore, it is critical to maintain the condition of S*/E < 3 in the reactor design [25].

From the FRC compression scaling laws [31] it is easy to conclude that wall compression will reduce S*/E while flux compression will lead to an increase of this parameter, and wall compression is the preferred method with stability consideration. However, real wall compression will consume the majority of the energy to compress the wall, since the wall mass is at least 3 orders of magnitude larger than the plasma mass, and therefore the plasma heating efficiency by real wall compression is very low. This difficulty is avoided in the FRC-MIF reactor design by a combination of FRC acceleration and effective wall compression in the conic tube. In this process, the wall is static and the compression is achieved by the kinetic energy. The S*/E parameters at each stage are listed in Table 1. It is seen that the effective wall compression in the conic tube reduces S*/E to a very small value of 0.7. This preconditioning is essential to ensure that the final S*/E parameter after magnetic compression is below the stability limit of 3.

### 3.2.7. Coil radius and efficiency of flux compression

From the FRC parameter design outlined in section 3.1, the FRC radius after compression is predetermined. From Fig. 7, it is seen that the white space between the coil and the FRC boundary is filled by magnetic field after flux compression. It is straightforward to see that the larger the coil radius, the more energy is required for the compression to fill the white space. Therefore, smaller coils will have higher flux compression efficiency; hence, the other important advantage of the conic tube is that, by reducing the plasma radius, the coil radius for the final magnetic compression is minimized.

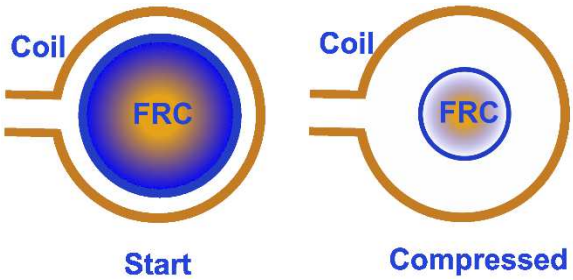



**Fig. 7. Schematic of FRC flux compression with fixed coil, showing that the white space between the coil and the FRC plasma boundary increases after compression. This white space is filled with magnetic energy during compression**

**4. Summary and discussion**

Unlike other MIF reactor designs [10,11], the new MIF reactor design is based on conservative FRC confinement scaling, and ignition can be achieved with a non-destructive magnetic field of 96.5 T. Therefore, it is possible to operate this fusion reactor repetitively — an essential feature required for practical fusion energy commercialization. Compared to similar FRC-MIF designs [33, 34], the design presented here has two unique features. First is the inclusion of the straight acceleration sections, which can provide a) sufficient plasma internal pressure before the final compression, and b) initial temperature control so that both plasma density and temperature can reach the design values after compression. Second is the adoption of metallic conic tubes for plasma precompression, which reduces S*/E to maintain tilt stability throughout the entire process. The conic tube also converts the kinetic energy obtained from acceleration to thermal energy, reduces the FRC plasma head-on collision speed to minimize collisional merging loss, and reduces the plasma radius for high efficiency magnetic compression.

Adiabatic compression heating requires that the compression time be shorter than the plasma confinement time. The FRC confinement time of 0.28 ms in the design provides adequate time for FRC formation, acceleration, and compression. The relatively long plasma and pulsed power interaction time is advantageous for effective energy coupling. The engineering difficulty is also significantly reduced compared to Z-pinch experiments, which requires plasma compression in the ns time scale [36].

When it comes to traditional adiabatic compression methods including flux compression and wall compression [31], it is very difficult to achieve ignition while maintaining stability. Flux compression deteriorates the FRC plasma stability, while real wall compression suffers from low plasma heating efficiency. The combination of FRC acceleration and the use of the conic metal tube for an effective wall compression offer a novel solution to these longstanding problems, paving the way for the first practical MIF reactor design.

Traditional wall compression has the advantage of improving the FRC stability [31]. However, real wall compression suffers from two difficulties. The mass of the metal liner is several orders of magnitude higher than the plasma mass, which absorbs a large fraction of the energy used for compression, lowering the plasma heating efficiency. It was estimated that a magnetic field on the order of 1000 T is required to achieve ignition with traditional wall compression method. When the metal liner is compressed and burnt, plasma will be contaminated by impurities. The combination of acceleration and compression of FRC plasma in a conic metal tube, which can be named as the effective kinetic wall compression, presents a novel alternative to the traditional wall compression method which solves the difficulties. The metallic conic tube is static during the compression which does not absorb the compression power, and no burning liner to contaminate the plasma. The compression work is done by the kinetic energy of FRC during acceleration. This effective kinetic wall compression method is possible due to the simple linear FRC geometry, and is potentially an important addition to the traditional flux compression and wall compression methods.

**Statements and Decalrations**

The author declares that a patent application (application number: 202610481542.8) related to the technology reported in this work has been filed with the patent office. The data that support the findings of this study are available from the corresponding author upon reasonable request.

## References


[1] J. Freidberg, Plasma Physics and Fusion Energy, Cambridge University Press (2013).

[2] A.J. Creely, M.J. Greenwald, S.B. Ballinger, et al., Overview of the SPARC tokamak. Journal of Plasma Physics 86, 865860502 (2020), doi: 10.1017/S0022377820001257.

[3] ASIPP and EUROfusion, BEST research plan, (EUROfusion 2025). https://euro-fusion.org/wp-content/uploads/2025/11/BEST-Research-Plan-v1.1.pdf.

[4] J. Wesson, Tokamaks, (Oxford Science Publications 2011).

[5] JET Team, Fusion energy production from a deuterium-tritium plasma in the JET tokamak. Nuclear Fusion 32, 187 (1992), doi: 10.1088/0029-5515/32/2/I01.

[6] S. E. Wurzel, S. C. Hsu, Progress toward fusion energy breakeven and gain as measured against the Lawson criterion. Physics of Plasmas 29, 062103 (2022), doi:10.1063/5.0083990.

[7] S. E. Wurzel, S. C. Hsu, Continuing progress toward fusion energy breakeven and gain as measured against the Lawson criteria. Physics of Plasmas 32, 112106 (2025), doi: 10.1063/5.0297357.
[8] H. Abu-Shawareb, R. Acree, P. Adams, et al., Achievement of target gain larger than unity in an inertial fusion experiment. Physical Review Letters 132, 065102 (2024), doi: 10.1103/PhysRevLett.132.065102.
[9] I. R. Lindemuth, R. E. Siemon, The fundamental parameter space of controlled thermonuclear fusion. American Journal of Physics 77, 407-416 (2009), doi: 10.1119/1.3096646.
[10] Benjamin Wang, Henry Fetsch, and Nathaniel J. Fisch, Long-pulse fast ignition in magnetized liner inertial fusion. Physical Review E 114, 015211 (2026), doi: 10.1103/ykf2-t49g.
[11] Timothée Nicolas, Christophe Goupil, Eric Herbert, Justin Ball, The Challenge for Adiabatically Heated FRC Based D-3He Fusion. Journal of Fusion Energy 45:24 (2026), doi: 10.1007/s10894-026-00565-z.
[12] D. N. Nguyen, J. Michel, C. H. Mielke, et al., Status and development of pulsed magnets at the NHMFL pulsed field facility. IEEE Transactions on Applied Superconductivity 26, 4300905 (2016), doi: 10.1109/TASC.2016.2515982.
[13] J. Béard, J. Billette, N. Ferreira, et al., Design and Tests of the 100-T Triple Coil at LNCMI. IEEE Transactions on Applied Superconductivity 28, 4300305 (2018), doi: 10.1109/TASC.2017.2779817.
[14] S. Zherlitsyn, B. Wustmann, T. Herrmannsdörfer, J. Wosnitza, Magnet-technology development at the dresden high magnetic field laboratory, Journal of Low Temperature Physics, 170, 447–451 (2013), doi: 10.1007/s10909-012-0764-7.
[15] J. Xie, S. Zhang, J. Shi, et al., Realisation of the reconfigurable pulsed high magnetic field facility and its scientific application at Wuhan National Pulsed High Magnetic Field Centre. High Voltage 8, 898–906 (2023), doi: 10.1049/hve2.12330.
[16] R. Battesti, J. Beard, S. Böser, et al., High magnetic fields for fundamental physics. Physics Reports 765, 1-39 (2018), doi: 10.1016/j.physrep.2018.07.005.
[17] M. Tuszewski, A. Smirnov, M.C. Thompson, et al., Field reversed configuration confinement enhancement through edge biasing and neutral beam injection. Physical Review Letters 108, 255008 (2012), doi: 10.1103/PhysRevLett.108.255008.
[18] K.F. McKenna, W.T. Armstrong, R.R. Bartsch, et al., Particle Confinement Scaling in Field-Reversed Configurations. Physical Review Letters 50, 1787-1790 (1983), doi: 10.1103/PhysRevLett.50.1787.
[19] M. Tuszewski, Field reversed configurations. Nuclear Fusion 28, 2033-2092 (1988), doi: 10.1088/0029-5515/28/11/008.
[20] N. Rostoker, M. W. Binderbauer, H. J. Monkhorst, Colliding Beam Fusion Reactor. Science 278, 1419-1422 (1997), doi: 10.1126/science.278.5342.14.
[21] D.P. Fulton, C.K. Lau, L. Schmitz, et al., Gyrokinetic simulation of driftwave instability in field-reversed configuration. Physics of Plasmas 23, 056111 (2016), doi: 10.1063/1.4948285.
[22] B.H. Deng, J.S. Kinley, K. Knapp, et al., Far infrared laser polarimetry and far forward scattering diagnostics for the C-2 field reversed configuration plasmas. Review of Scientific Instruments 85, 11D401 (2014), doi: 10.1063/1.4884903.
[23] M.W. Binderbauer, H. Guo, M. Tusaewski, et al., Dynamic formation of a hot field reversed configuration with improved confinement by supersonic merging of two colliding high-□ compact toroids. Physical Review Letters 105, doi:10.1103/PhysRevLett.105.045003 (2010).
[24] M.W. Binderbauer, T. Tajima, L.C. Steinhauer, A high performance field-reversed configuration. Physics of Plasmas 22, 056110 (2015), doi: 10.1063/1.4920950.
[25] E. V. Belova, R. C. Davidson, H. Ji, M. Yamada, Advances in the numerical modeling of field-reversed configurations. Physics of Plasmas 13, 056115 (2006); doi: 10.1063/1.2179426.
[26] A.C. Kolb, W.H. Lupton, R.C. Elton, et al., “Plasma confinement, heating and losses in PHAROS with an extended current pulse” in Plasma Physics and Controlled Nuclear Fusion Research (Proc. 2nd Int. Conf., Culham, 1965), 1, IAEA, Vienna, 261-273 (1966).
[27] W.T. Armstrong, R.K. Linford, J. Lipson, D.A. Platts, E.G. Sherwood, Field-reversed experiments (FRX) on compact toroids. Physics of Fluids 24, 2068-2089 (1981), doi:10.1063/1.863303
[28] M. Tuszewski, A semiempirical formation model for field reversed configurations. Physics of Fluids 31, 3754–3759 (1988), doi: 10.1063/1.866894.

[29] A. L. Hoffman, Richard D. Milroy, John T. Slough, and Loren C. Steinhauer, Formation of Field-Reversed Configurations Using Scalable, Low-Voltage Technology. Fusion Technology 9, 48-57 (1986), doi: 10.13182/FST86-A24700.
[30] G. Votroubek, J. Slough, S. Andreason, C. Pihl, Formation of a Stable Field Reversed Configuration through Merging. Journal of Fusion Energy 27, 123–127 (2008), doi: 10.1007/s10894-007-9103-4.
[31] R. L. Spencer, M. Tuszewski, R. K. Linford, Adiabatic compression of elongated field-reversed configurations. Physics of Fluids 26, 1564-1568 (1983), doi: 10.1063/1.864334.
[32] E.V. Belova, S.E. Clark, R. Milroy, G. Votroubek, A. Pancotti, D. Kirtley, Hybrid simulations of FRC merging and compression. Fusion Science and Technology (2025), doi: 10.1080/15361055.2025.2546290.
[33] J. Slough, G. Votroubek, C. Pihl, Creation of a high-temperature plasma through merging and compression of supersonic field reversed configuration plasmoids. Nuclear Fusion 51, 053008 (2011), doi: 10.1088/0029-5515/51/5/053008.
[34] J. Slough, A compact fusion reactor based on the staged compression of a field reversed configuration. Nuclear Fusion 65, 106019 (2025), doi: 10.1088/1741-4326/ae034d.
[35] Elena V. Belova, Ronald C. Davidson, Hantao Ji, and Masaaki Yamada, Kinetic effects on the stability properties of field-reversed configurations. II. Nonlinear evolution. Physics of Plasmas **11**, 2523 (2004), doi: 10.1063/1.1666293.
[36] Stephen A. Slutz, and Matthew R. Gomez, Fusion gain from cylindrical liner-driven implosions of field reversed configurations. Phys. Plasmas **28**, 042707 (2021); https://doi.org/10.1063/5.0044919.